JOURNAL OF SOLID STATE CHEMISTRY 87, 331–343 (1990)

Microstructural Characterization of the Fluorite Phase in the U–La–O System. I. Rhombohedral Microdomain Formation in $(U_{1-y}La_y)O_{2\pm x}$, $0.56 \leq y \leq 0.67$

P. HERRERO, P. GARCIA-CHAIN, AND R. M. ROJAS[1]

Instituto de Ciencia de Materiales, CSIC, Serrano 113, 28006 Madrid, Spain

Received August 9, 1989; in revised form March 12, 1990

A series of hyperstoichiometric, stoichiometric, and hypostoichiometric U–La mixed oxides with fluorite-type structures has been prepared in air at 1673 K in the composition range $(U_{1-y}La_y)O_{2\pm x}$, $0.33 \leq y \leq 0.67$, by a mixed organic precursor/ceramic procedure. The oxidation state of uranium in these materials has been examined by XPS and near FT-IR spectroscopy, uranium ions existing within each sample either as U^{5+} and U^{6+} ($0.33 \leq y \leq 0.50$) or U^{6+} and U^{4+} ($0.56 \leq y \leq 0.67$). Electron diffraction studies reveal two sets of patterns with diffuse scattering phenomena depending on composition. The diffuse scattering for specimens with $0.56 \leq y \leq 0.67$ is discussed in terms of microdomain formation of a rhombohedral R_{III} phase, that is obtained as a single phase when samples with these compositions were annealed at 1373 K for 100 hr.

Introduction

Research into the fundamentals and properties of nonstoichiometric fluorite-type materials has attracted the attention of many solid state chemists and physicists due to their technological interest. Many of them exhibit anionic conductivity properties making them potentially important in the material context as electrolytes or electrodes for solid state batteries and fuel cells, oxygen sensors, lasers, etc. (*1–4*). Experimental studies carried out during the last few years have revealed the structural complexity of these materials, in which the varying states of defects ordering both in the anionic and cationic sublattices give rise to the formation of clusters, short-range order throughout the structure, ordered microdomains, etc., and finally can lead to the formation of new structures (*5–10*).

Fluorite phase formed in the UO_2–Ln_2O_3 systems constitutes a group of urania-based mixed oxides that are able to support large deviations from stoichiometry. Among them, the U–La–O system has been extensively studied because of its interest in nuclear fuel technology (*11–14*). The phase diagram for the pseudobinary UO_2–$LaO_{1.5}$ system indicates the formation of the fluorite phase $(U_{1-y}La_y)O_{2\pm x}$ in the composition range $0.26 \leq y \leq 0.80$ at temperatures higher than 1623 K, as well as the existence of three rhombohedral ordered phases, R_I, R_{II}, and R_{III} (*15, 16*). The crystal structure of the R_I phase La_6UO_{12}, isostructural to Y_6UO_{12} and Lu_6UO_{12}, has been determined by X-ray powder diffraction technique (*17*). The or-

[1] To whom correspondence should be addressed.

0022-4596/90 $3.00

TABLE I

CELL PARAMETER VALUES FOR THE R_{III} PHASE

Hexagonal cell parameters	Rhombohedral cell parameters	y value in $U_{1-y}La_yO_{2\pm x}$	Ref.
a_H = 1.573 nm	a_R = 1.104 nm	0.60	(*18*)
c_H = 1.881 nm	α = 90.90°		
a_H = 1.580 nm	a_R = 1.109 nm	0.61	(*15*)
c_H = 1.891 nm	α = 90.87°		
a_H = 0.394 nm	a_R = 0.667 nm	0.57	(*19*)
c_H = 1.880 nm	α = 34.38°		
a_H = 0.393 nm	a_R = 0.386 nm	0.60	(*12*)
c_H = 0.938 nm	α = 61.18°		
a_H = 0.393(1) nm	a_R = 0.669 nm	0.60	This work
c_H = 1.890(4) nm	α = 34.10°		

dered R_{II} phase, stable up to 1593 K, exists in a narrow range of composition, $0.73 \leq y \leq 0.76$, and its phase width decreased with temperature. The X-ray powder pattern can be indexed on the hexagonal system, with cell parameters very close to the R_I phase. A third ordered R_{III} phase is found below 1493 K, with phase width ranging from $0.55 \leq y \leq 0.67$. The X-ray diffraction diagram of this phase has been indexed on the basis of a hexagonal cell, but different cell parameters have been reported (Table I).

Within the scope of the reinvestigation we are currently carrying out on the U–La–O system, we have undertaken the microstructural study of the fluorite phase formed in the $(U_{1-y}La_y)O_{2\pm x}$ mixed oxide at 1673 K in air, in the composition range $0.33 \leq y \leq 0.67$, in which hyper, nearly stoichiometric and slightly hypostoichiometric phases are formed. The evolution of the oxidation state of uranium with composition determined by X-ray photoelectron and near FT-IR spectroscopy seems to be closely related to the formation of microdomains detected by TEM in these materials.

Experimental

Sample preparation. A series of U–La-mixed oxides $(U_{1-y}La_y)O_{2\pm x}$ ($0.33 \leq y \leq 0.67$) were prepared by a mixed ceramic/organic precursor method (*20*). Stoichiometric amounts of lanthanum uranyl propionate and uranium trioxide or lanthanum sesquioxide were ground together and ignited at 1073 K. The mixtures were then calcined at 1673 K in air in platinum containers for 150 hr and quenched on a metalic plate. Samples quenched from 1673 K were subsequently annealed at 1373 K for 100 hr and then quenched by rapidly removing them from the furnace. A batch of the annealed P-7 sample was also heated at 1673 K for 14 hr and then quenched.

X-ray diffraction. X-ray powder diffraction patterns were recorded on a Siemens D-500 diffractometer with monochromatized Cu$K\alpha$ radiation and W as internal standard. Diagrams were scanned at 1/5° $2\theta \cdot \text{min}^{-1}$ and lattice parameters determined by a routine least-squares procedure applied to the diffraction lines above $2\theta = 40°$.

Determination of the oxygen content. The oxygen content of these samples was determined by a back-titration method (*21, 22*). About 50 mg of sample was dissolved in a pipetted excess of cerium (IV) sulfate solution to which several milliliters of 3 M H_2SO_4 were added. The excess Ce (IV) was titrated against standard iron (II) ammonium sulfate solution with ferroin indicator.

Thermal analysis. Thermal stability of these materials up to 1673 K was investigated using Stanton STA 781 equipment. A programmed heating/cooling rate of 10° · min^{-1} and still or dynamic air (50 ml · min^{-1}) were used. About a 70-mg sample was used in each run and sensitivities of 80 μV and 10 mg for differential thermal analysis (DTA) and thermogravimetric (TG) curves, respectively, were selected.

Infrared spectroscopy. FT-IR spectra were recorded on a Nicolet 60 SX spectrometer, in the near IR region (4000–10,000 cm^{-1}) in the diffuse reflectance mode, and 5000 spectra accumulations.

Magnetic susceptibility. Magnetic susceptibility was measured by the Faraday method in the temperature range 5 K to room temperature. The apparatus was calibrated with $Hg[Co(CN)_4]$ as standard. The diamagnetic contributions were corrected as follows (*23*): La^{3+}, 20×10^{-6} cgs; O^{2-}, 12×10^{-6} cgs; U^{4+}, 35×10^{-6} cgs; U^{5+}, 26×10^{-6} cgs; U^{6+}, 19×10^{-6} cgs.

X-ray photoelectron spectroscopy. X-ray photoelectron spectra were recorded in an ESCA Leybold-Heraeus Model LHS-10 photoelectron spectrometer with Mg$K\alpha$ radiation, in the pass energy mode at 50 eV. Calibration was achieved using the Cls peak at 284.6 eV and samples were examined in the form of pellets.

Electron microscopy. Electron diffraction and microscopy were carried out on a Siemens Elmiskop 102 and Jeol 200 FX microscopes, both equipped with a ±45° goniometer stage. Samples for study were crushed in an agate mortar and suspended in acetone, then transferred to holey carbon-coated copper grids.

Results

X-ray diffraction and O/M ratio. X-ray diffraction analysis revealed that the U–La-mixed oxides quenched from 1673 K are single phase compounds having the fluorite-type structure over the whole composition range. Composition and lattice parameters are gathered in columns 2 and 3 of Table II. Cell parameters increased linearly from samples P-1 to P-4 and P-6 to P-9, as shown in Fig. 1.

X-ray data recorded on the annealed materials indicate that for samples P-1 to P-4 the fluorite structure is preserved, although a large broadening of the Bragg peaks occurs on annealing (Figs. 2a and b). Diagrams of annealed P-6 to P-9 could be indexed on the basis of the rhombohedral R_{III} phase (*15*), with cell parameters ranging from a_H = 1.576(3) nm, c_H = 1.881(5) nm (P-6) to a_H = 1.577(1) nm, c_H = 1.897(2) nm (P-9). The corresponding rhombohedral parameters are a_R = 1.105 nm, α = 90.97° and a_R = 1.108 nm, α = 91.08°, respectively, which implies that the R_{III} phase could be considered as a double distorted fluorite structure. However, the X-ray patterns can also be indexed with smaller cell parameters, a_H = .393(1) nm, c_H = 1.890(4) nm (P-7), a_R = .669 nm, α = 34.10° (Fig. 3b) close to those reported by Kovba (*19*). This cell may also be referred to a rhombohedral unit cell derived from a double fluorite (*40*). Parameters reported by Tagawa *et al.* (*12*) do not allow the indexing of the weaker reflections observed in our diagrams. The X-ray diagram of sample P-5, with composition $(U_{0.5}La_{0.5})O_{2\pm x}$, indicates that a mixture of both fluorite and R_{III} phases is formed after annealing.

Oxygen content as deduced from back-titration data is indicated in column 2 of Table II. The oxygen to metal ratio O/M (M = U + La), (Fig. 4) decreases dramatically with increasing y for samples P-1 to P-6, but diminishes less rapidly for samples with higher lanthanum content. At the same time, the mean valency of uranium increases with the lanthanum concentration y, as shown in Fig. 5. From these data it follows that uranium in these mixed oxides has to be in at least two different oxidation states, most

TABLE II

CELL PARAMETERS AND PROPOSED FORMULATION FOR THE FLUORITE PHASES QUENCHED FROM 1673 K

Sample	Composition	Cell parameter a(nm)	Formulation
P-1	$U_{0.67}La_{0.33}O_{2.20}$	0.54844(1)	$U^{5+}_{0.62}U^{6+}_{0.05}La_{0.33}O_{2.20}$
P-2	$U_{0.64}La_{0.36}O_{2.18}$	0.54920(2)	$U^{5+}_{0.56}U^{6+}_{0.08}La_{0.36}O_{2.18}$
P-3	$U_{0.60}La_{0.40}O_{2.14}$	0.55021(2)	$U^{5+}_{0.52}U^{6+}_{0.08}La_{0.40}O_{2.14}$
P-4	$U_{0.56}La_{0.44}O_{2.11}$	0.55125(3)	$U^{5+}_{0.48}U^{6+}_{0.08}La_{0.44}O_{2.11}$
P-5	$U_{0.50}La_{0.50}O_{2.04}$	0.55212(3)	$U^{5+}_{0.42}U^{6+}_{0.08}La_{0.50}O_{2.04}$
P-6	$U_{0.44}La_{0.56}O_{1.99}$	0.55284(1)	$U^{4+}_{0.17}U^{6+}_{0.27}La_{0.56}O_{1.99}$
P-7	$U_{0.40}La_{0.60}O_{1.98}$	0.55385(2)	$U^{4+}_{0.12}U^{6+}_{0.28}La_{0.60}O_{1.98}$
P-8	$U_{0.36}La_{0.64}O_{1.97}$	0.55477(4)	$U^{4+}_{0.07}U^{6+}_{0.29}La_{0.64}O_{1.97}$
P-9	$U_{0.33}La_{0.67}O_{1.96}$	0.55533(4)	$U^{4+}_{0.05}U^{6+}_{0.28}La_{0.67}O_{1.96}$

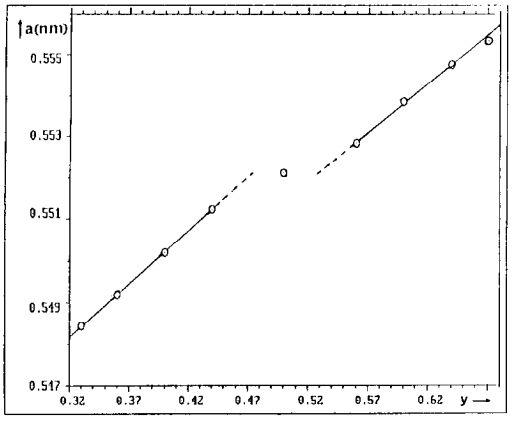

FIG. 1. Lattice parameter variation as a function of y, in the cubic fluorite phase $(U_{1-y}La_y)O_{2\pm x}$ quenched from 1673 K in air.

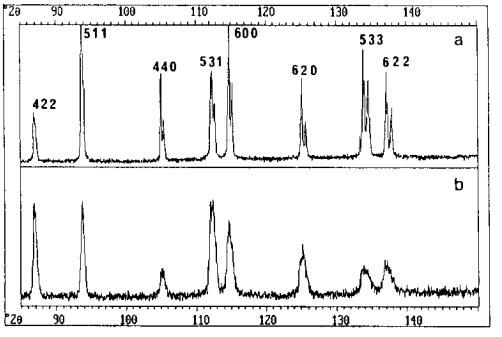

FIG. 2. X-ray diffraction patterns of sample P-2: (a) quenched from 1673 K; (b) annealed at 1373 K.

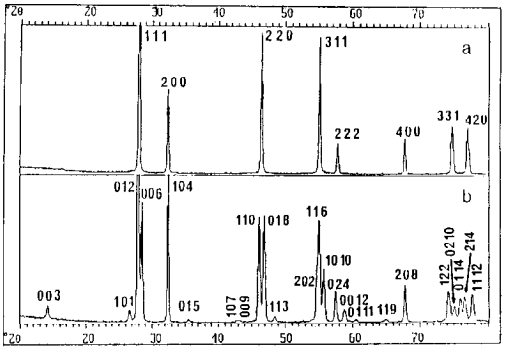

FIG. 3. X-ray diffraction patterns of sample P-7: (a) quenched from 1673 K; (b) annealed at 1373 K.

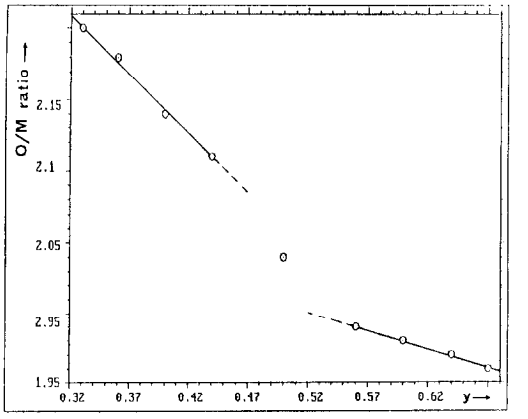

FIG. 4. Oxygen to metal ratio as a function of y, in $(U_{1-y}La_y)O_{2\pm x}$ quenched from 1673 K in air.

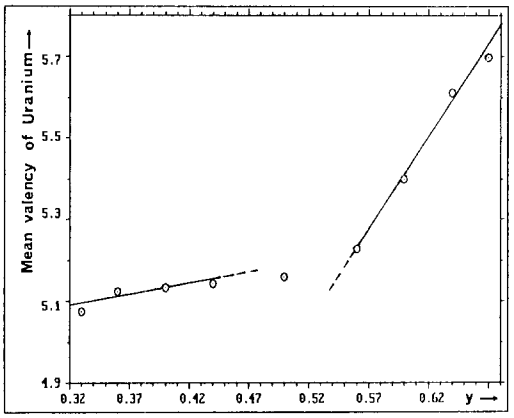

FIG. 5. Mean valency of uranium as a function of y, in $(U_{1-y}La_y)O_{2\pm x}$ quenched from 1673 K in air.

probably U(IV) or (V) and U(VI). The existence of U(V) in these materials cannot be discarded since it is stabilized in solid compounds, specially ternary mixed oxides (*24–26*). In order to elucidate oxidation states of uranium in these materials, XPS and near FT-IR spectra were recorded.

XPS and near FT-IR spectroscopy. X-ray photoelectron spectra of 4*f* and valence band regions, recorded on samples P-1, P-5, P-7, and P-9, are depicted in Figs. 6 and

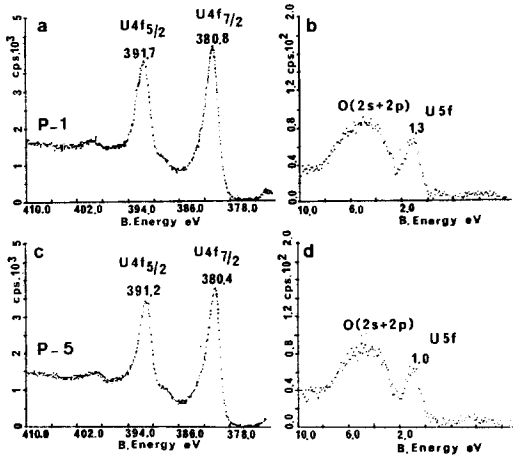

FIG. 6. X-ray photoelectron spectra of fluorite samples (P-1): (a) U4*f*, (b) valence band region; (P-2): (c) U4*f*, (d) valence band region.

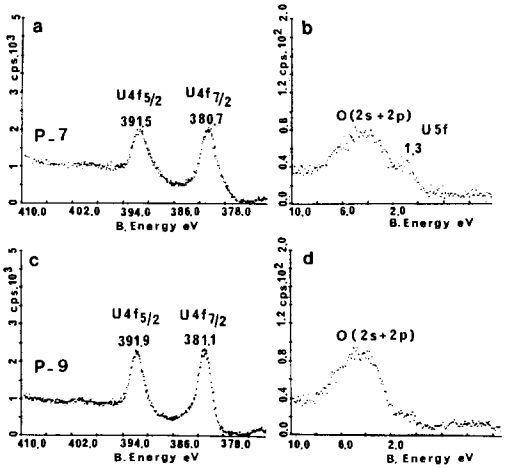

FIG. 7. X-ray photoelectron spectra of fluorite samples (P-7): (a) U4*f*, (b) valence band region; (P-9): (c) U4*f*, (d) valence band region.

7. Binding energies measured for the $U4f_{5/2,7/2}$ and U5*f* photoelectron peaks are gathered in Table III, in which our measurements are compared with those reported for some analogous materials. Binding energies for UO_2, UO_3, and U_3O_8 have also been listed. A close correspondence cannot be assumed since values reported by different authors differ for a given compound by about 1 eV (*27*). Moreover there are a number of factors that contribute to measured binding energies, not the least of which are changes in uranium coordination number and consequently changes in structure and bond lengths (*28*). Nevertheless, binding energies measured for samples P-1, P-5, and P-7 are within the values reported for some related compounds in which the existence of U(V) has been claimed (*25, 27, 29*). For sample P-9, the U4*f* core levels are slightly shifted to higher energies, being identical to the reported values for U_3O_8 (*28–30*). A satellite structure at 7.9 eV to the high binding energy side of the $U4f_{5/2,7/2}$ doublet is clearly observed in spectra recorded on samples P-1 and P-5. Similar satellite struc-

TABLE III

BINDING ENERGIES (EV) FOR THE U4$f_{5/2,7/2}$ AND U5f PEAKS OF SAMPLES P-1, P-5, P-7, AND P-9 AND REPORTED BINDING ENERGIES FOR UO_2, UO_3, U_3O_8, AND SOME URANIUM MIXED OXIDES

Sample	$4f_{5/2}$	Satellite	$4f_{7/2}$	Satellite	$5f$	Refs.
$U_{0.67}La_{0.33}O_{2.20}$ (P-1)	391.7	7.9	380.8	7.9	1.3	This work
$U_{0.50}La_{0.50}O_{2.04}$ (P-5)	391.2	7.9	380.4	7.9	1.0	This work
$U_{0.40}La_{0.60}O_{1.98}$ (P-7)	391.5	—	380.7	—	1.3	This work
$U_{0.33}La_{0.67}O_{1.96}$ (P-9)	391.9	—	381.1	—	—	This work
UO_2	390.95	—	380.15	—	—	(*31*)
U_3O_8	391.9	—	381.1	7.8	1.3	(*28, 30*)
γ-UO_3	392.95	—	382.0	—	—	(*35*)
$U^{V}Sb_3O_{10}$	392.3	7.9	381.3	—	—	(*29*)
$U^{V}Nb_3O_{10}$	—	—	380.0	—	—	(*36*)
$U^{VI}La_2O_6$	—	—	381.9	—	—	(*27*)
$U^{VI}_{0.40}La_{0.60}O_2$	—	—	381.0	—	—	(*27*)
$U^{V}_{0.50}La_{0.50}O_2$	—	—	380.9	—	—	(*27*)
$U^{V}_{0.75}La_{0.25}O_2$	—	—	380.9	—	—	(*27*)

ture has been considered by several authors as an argument for U(V) (*24, 25, 29*) and it would be in favor of the existence of uranium in this oxidation state in samples with $0.33 \leq y \leq 0.50$.

The valence region shows a steady decrease in U5f intensity compared to the U–O2p "bonding band" (*31*) ongoing from sample P-1 to P-9, where the U5f signal is hardly observed.

From both the core level and satellite position, significant amounts of U(V) can be recognized in samples P-1 and P-5, whereas in sample P-7, without appreciable satellite structure, the U5f signal would be originated by a certain amount of uranium (IV). On the other hand, the systematic decrease of the U5f intensity (*31*) clearly indicates that the oxidation state of uranium increases from sample P-1 to P-9 in which most uranium would be as U(VI), $5f^{\circ}$ outer electronic configuration.

Near FT-IR spectra recorded in the 5000–7000 cm^{-1} range are depicted in Fig. 8. They provide more conclusive evidence about the oxidation state of uranium in these materials. A band centered at 6610 cm^{-1} is clearly seen in the reflectance spectra corresponding to samples P-1 to P-5, while spectra recorded on samples P-6 to P-9 do not show any significant feature in this region. A band at almost the same frequency has been observed in the reflectance spectra of some uranium (V) mixed oxides with fluorite- or perovskite-type structures (*32*) that seem to be characteristic of uranium (V) (*33*). Therefore, it can be inferred that samples with composition ranging between $0.33 \leq y \leq 0.50$ (P-1 to P-5) have a significant amount of U(V), while oxidation states of uranium in samples P-6 to P-9 ($0.56 \leq y \leq 0.67$) have to be another than U(V). These results agree with plots shown in Figs. 1, 4, and 5 from which it is evident that samples can be grouped together in two different sets: P-1 to P-4 and P-6 to P-9; whereas sample P-5 does not fit within either of these two sets. It would indicate that this particular sample constitutes a singular point in the series, that it is stated by its characteristic behavior on annealing. From all the above indicated, the formulation listed in column

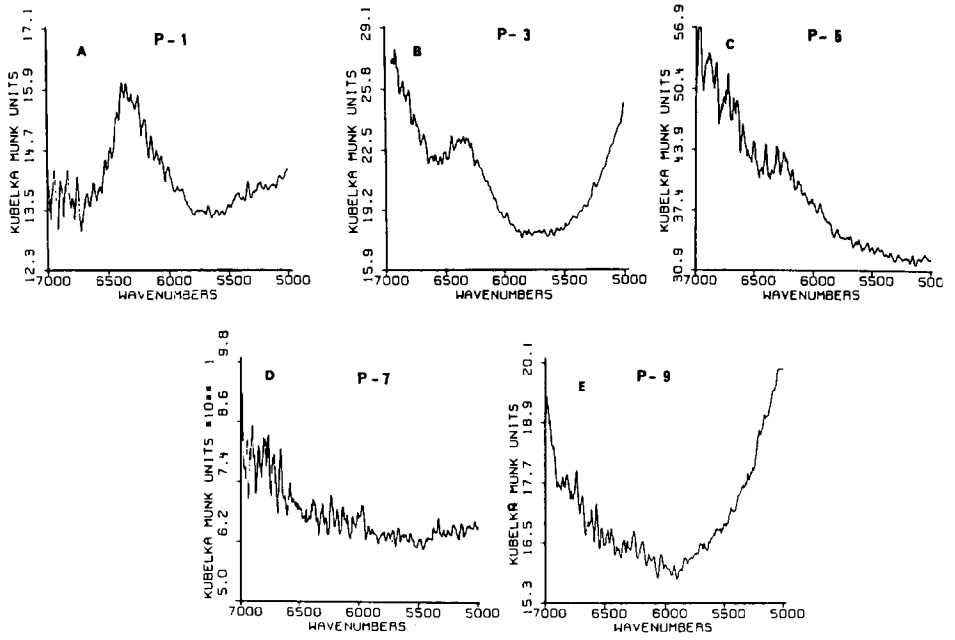

FIG. 8. Near FT-IR spectra of fluorite samples: (A) P-1, (B) P-3, (C) P-5, (D) P-7, (E) P-9.

4 of Table II is proposed for mixed U–La oxides with fluorite-type structure, in which hyperstoichiometric, nearly stoichiometric, and hypostoichiometric compositions occur.

Magnetic measurements. Magnetic susceptibility vs temperature curves for samples P-1, P-5, and P-8 are presented in Fig. 9.

The magnetic susceptibility obeys the Curie–Weiss law in the whole temperature range, i.e., from 5 K to room temperature. The effective Bohr magneton number estimated from reciprocal magnetic susceptibility vs temperature plots ranges from 1.38 μ_B for sample P-1 to 0.73 μ_B for a sample with composition $U_{0.36}La_{0.64}O_{1.97}$ (P-8). These values are lower than those observed in some uranates of alkaline-earth elements with fluorite structure MU_2O_6 (M = Ca, Sr, Ba) (1.68–1.82 μ_B) in which the uranium is supposed to be as U(V) (*34*); nevertheless our values are close, up to sample P-5 (1.06 μ_B), to those recently reported for CaU_2O_6 (1.3 μ_B). CdU_2O_6 (1.2 μ_B), and YUO_4 (1.1–0.9 μ_B) (*25*). The compound with $y = 0.67$ (P-9) exhibits very small magnetic susceptibility, suggest-

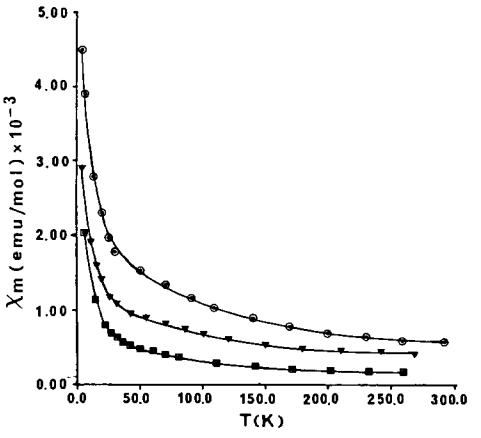

FIG. 9. Magnetic susceptibilities of fluorite samples: (⊙) P-1, (▼) P-5, (⊡) P-8.

ing that uranium ion exists in the diamagnetic Rn ($5f^0$) hexavalent state.

Antiferromagnetic interaction is not observed either for the mixed oxides having excess oxygen (P-1 to P-5) or for the slightly hypostoichiometric compositions (P-6 to P-8). In the former case it can be explained if the excess oxygen would be located at intersticial sites of the fluorite structure, weakening or hindering magnetic interactions between paramagnetic ions (*14*). For lanthanum richer samples ($0.56 \leq y \leq 0.64$) it is likely that diamagnetic La^{3+} cations intercept the magnetic interactions (*25*), and in this way dilute the paramagnetic cationic lattice, since uranium is the minor component in these P-6 to P-8 mixed oxides.

Thermal stability. When samples were submitted to programmed heating and cooling cycle, from room temperature up to 1673 K, in dynamic or still air atmospheres, differential thermal analysis (DTA) curves did not show any endothermal or exothermal effect. Significant weight variations were not observed in the thermogravimetric (TG) curves (*20*). Moreover, X-ray powder diagrams recorded on each sample after and before thermal analyses were almost identical. However, X-ray data of annealed materials indicated that samples P-6 to P-9 experiment a cubic $\Rightarrow$ rhombohedral transformation on annealing. It follows that this transformation must be a slow process that requires long annealing periods in order to achieve a complete reordering of the lattice.

Electron diffraction and microscopy. Representative selected area diffraction patterns for nonannealed samples in the [$\bar{1}$10] zone axis are presented in Fig. 10. They clearly show, in addition to the diffraction maxima corresponding to the reciprocal lattice of the fluorite cell, a number of diffuse scattering phenomena. Three sets of patterns can be distinguished:

(a) diffuse spots lying at about 1/3 and 2/3 of the ⟨111⟩ fluorite direction and equivalent ones. They also present diffuse maxima at (011) and (100). Samples P-1 to P-3 (Fig. 10a).

(b) diffuse spots also lying along the ⟨111⟩ direction and equivalent ones but located at (1/2 1/2 1/2). Samples P-6 to P-9 (Fig. 10b).

(c) without any significant diffuse features. Samples P-4 and P-5 (Fig. 10c).

Diffuse maxima are also present in other zone axes; Figure 10d shows a pattern corresponding to sample P-1 in the [11$\bar{2}$] zone axis. Other zones show so weak diffuse phenomena that it is not possible to build up a complete geometric reciprocal lattice. Figure 11a shows the direct image corresponding to sample P-7 $(La_{0.6}U_{0.4})O_{1.99}$ along the $\langle 110 \rangle_F$. Fringes corresponding to the $(111)_F$ planes of the fluorite can be observed with a certain disorder characteristic of this material. Areas marked A and B, where a doubling along the $\langle 111 \rangle_F$ is observed, do not exactly correspond to the fluorite phase, and they could be interpreted as microdomains of a new phase coherently intergrown within the fluorite matrix. In the image shown in Fig. 11b, obtained on sample P-7 after 14 hr annealed at 1373 K, well-defined microdomains of the R_{III} phase could be identified. From this picture, the hexagonal c_H parameter of the R_{III} cell can be unequivocally determined, being $c_H = 1.890(4)$ nm. From the measured $d(010) = 0.34$ nm interplanar space, $a_H = 0.393(1)$ nm is obtained; the X-ray pattern being completely indexed with these parameters (Fig. 3b). However, the resolution of the image is not good enough to assure the true a_H value; additional HRTEM imaging work is currently being done.

TEM studies on samples annealed at 1373 K indicate that significant differences occur in their electron diffraction patterns: diffuse spots convert into sharp reflections occupying the same positions. This effect

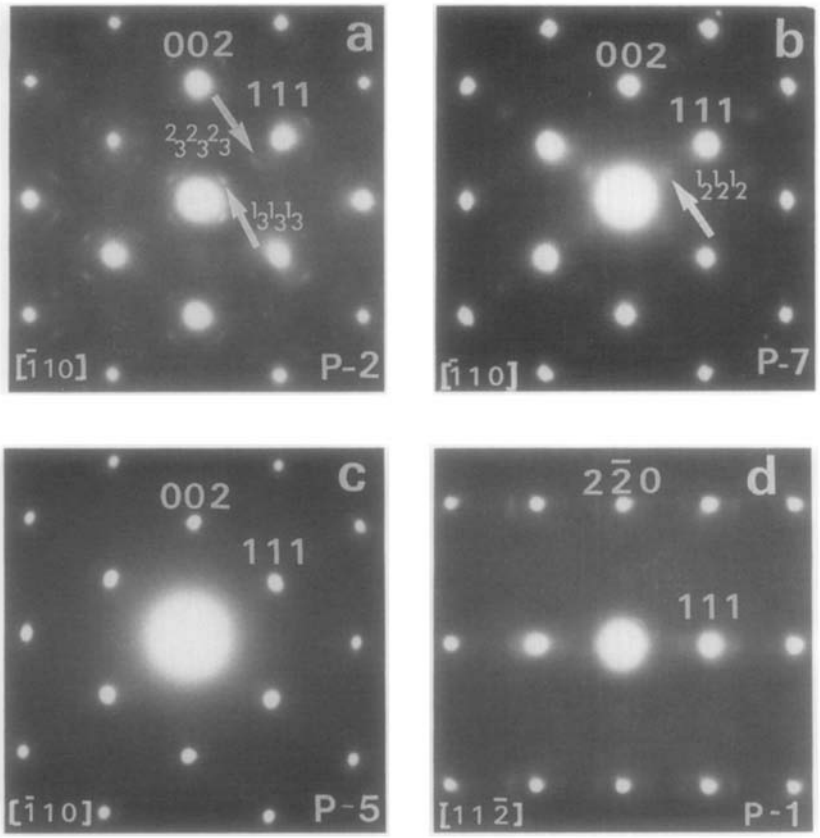

FIG. 10. Representative selected area electron diffraction patterns for samples with the fluorite-type structure. (a, b, and c) along the [$\bar{1}$10] zone axis; (d) along the [11$\bar{2}$] zone axis.

is illustrated in Figs. 12a and 12b that show the electron diffraction patterns corresponding to samples P-7 and P-2, respectively. For sample P-7, the pattern can be indexed on the basis of a double fluorite cell with $a \approx 2a_F$ or, more accurately and according to X-ray and TEM results, on the basis of the R_{III} rhombohedral cell with the hexagonal parameters above indicated.

Figure 12b, case of sample P-2, shows a more complicated situation. X-ray data indicates that the fluorite-type structure is preserved after annealing (see Fig. 2b); however, electron diffraction diagrams indicate a possible tripling of the original cell. We are actually performing a more detailed structural study on annealed P-1 to P-3 samples.

Discussion

Although a random distribution of lanthanum and uranium ions occupying eight coordinated sites at the fluorite lattice may be deduced from X-ray data, the presence of diffuse maxima in electron diffraction patterns indicate the existence of some kind of structural alterations in which both cations would be involved. In general, diffuse scattering phenomena observed in fluorite-related systems (*7, 37–39*) has been interpreted with crystallographic models ranging

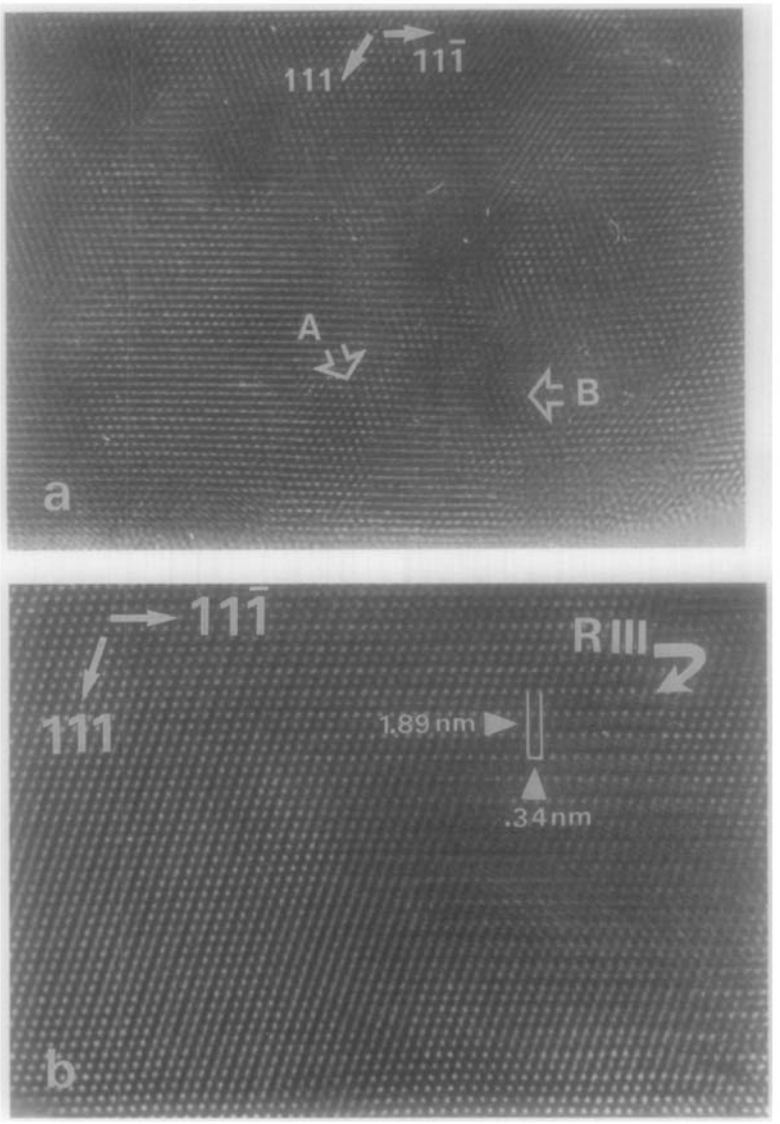

FIG. 11. Electron micrograph of the fluorite sample P-7 along the [$\bar{1}$10] zone axis: (a) showing fringes corresponding to $(111)_F$ planes and irregular features in periodicity, areas A and B; (b) after 14 hr of annealing.

from statistical descriptions of homogeneous short-range order of ions or vacancies to the concept of fully ordered microdomains that exit coherently within a disordered matrix and which allow a slightly heterogeneous distribution of ions.

The diffuse scattering detected in the U–La–O series is characteristic of oxides with defect fluorite structure and closely resembles that found in the $(Tb_xGd_{1-x})_2ZrO_{7+y}$ (*7*) or $Ca_xM_{1-x}O_{2-x}$ (M = Zr, Hf) (*38*) system. In both cases it has been attributed to the existence of microdomains of pyrochlore structure in the former case, or of

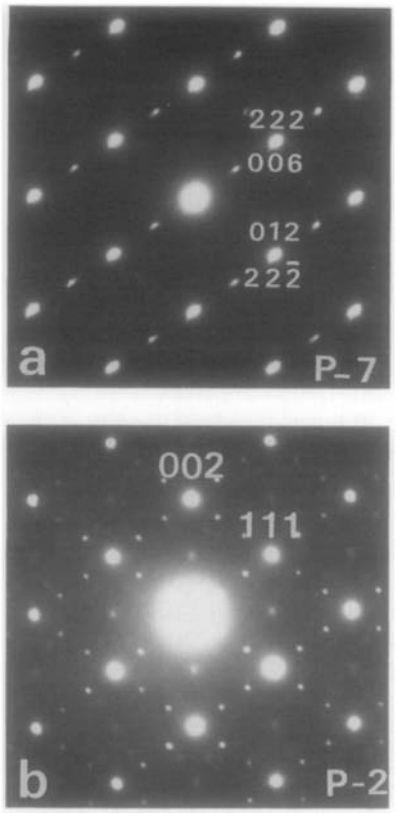

FIG. 12. Electron diffraction patterns corresponding to annealed samples: (a) P-7, zone axis $[\bar{1}10]_C \| [100]_H$; and (b) P-2 along $[\bar{1}10]_C$; C and H stand for cubic and hexagonal, respectively.

$CaZr_4O_9$ in the latter, embedded coherently within the cubic matrix. A prolonged annealing of these materials gave place to entirely ordered structures; their electron diffraction diagrams showing sharp spots lying at the same positions that were occupied by diffuse maxima. It is also worth mentioning that those diffuse maxima do not change their geometrical features (position, size, and form) with variation in the composition. In our case, as we already noted, two sets of patterns with diffuse phenomena can be distinguished and within each set the geometric features keep practically unaltered. This could indicate two different types of ions ordering on both groups.

According to X-ray and TEM results, diffuse scattering in fluorite samples P-6 to P-9 may then be explained by the formation of ordered zones of R_{III} microdomains residing in a coherent way within the fluorite matrix. The images depicted in Fig. 11 support this assumption and areas A and B in Fig. 11a may therefore be interpreted as zones of material in different stages of the fluorite $\Rightarrow$ R_{III} transformation, that probably implies a doubling of the fluorite cell as an intermediate step in such a transformation. On annealing, microdomains keep growing till the ordered R_{III} phase is obtained as a single phase.

A plausible explanation for the formation of microdomains of the rhombohedral phase in samples P-6 to P-9 can be made if we pay attention to the amount of U^{6+} present in the fluorite phase (Table II) and the ionic radii of the cationic species (*39*):

$$^{VIII}La^{3+} = 0.116 \text{ nm} \quad ^{VIII}U^{4+} = 0.100 \text{ nm}$$
$$^{VII}U^{5+} = 0.096 \text{ nm} \quad ^{VII}U^{6+} = 0.088 \text{ nm}$$

It is evident that U^{6+} is too small to be accommodated within an undistorted cubic surrounding of oxygens (*41*). Therefore, it is not unlikely to suppose that a readjustment of the nearest and next-nearest neighbors occurs, resulting in a distortion of the coordination polyhedra around U^{6+} in an ordered way. This would give rise to the formation of microdomains with trigonal symmetry, that cause the observed diffuse scattering. A prolonged annealing leads to the total arrangement of the ions giving place to the formation of the R_{III} superstructure. Nevertheless the reverse $R_{III} \Rightarrow$ fluorite (order $\Rightarrow$ disorder) transformation that would give place to a truly randomly disordered structure cannot be completely attained on heating at 1673 K, and microdomains of the R_{III} phase are always present, causing the diffuse scattering observed on samples P-6 to P-9 quenched from 1673 K.

For samples P-1 to P-3 a similar but not identical situation must occur since diffuse

maxima differ in number and position indicating a possible tripling of the fluorite cell. Moreover, in this case we are dealing with hypostoichiometric fluorite phases and the anion excess must also play a significant role. The absence in these compounds of significant amounts of U^{6+} as well as lower lanthanum contents would prevent the distortion of the coordination polyhedra and consequently favors, according to the X-ray results, the apparent stabilization of the fluorite phase.

In samples P-4 and P-5 where no diffuse phenomena are detected, the situation must correspond to a statistical disordered lattice with La and U ions occupying random positions.

Acknowledgments

We thank Dr. González Calbet for his valuable comments and Mr. Garcia Delgado for technical assistance with electron microscopes. We also acknowledge Dr. A. R. González-Elipe and the University of Sevilla for the facilities in recording the XPS spectra.

References

1. T. H. Estell and S. N. Flengas, *Chem. Rev.* **70,** 339 (1970).
2. T. Takahashi, *in* "Physics of Electrolytes" (J. Hladik, Ed.), Vol. 2, Academic Press, London (1972).
3. R. M. Dell and A. Hooper, *in* "Solid Electrolytes" (P. Hagenmuller and W. van Gool, Eds.), p. 291, Academic Press, San Diego (1978).
4. J. M. Reau and J. Portier, *in* "Solid Electrolytes" (P. Hagenmuller and W. van Gool, Eds.), p. 312, Academic Press, San Diego. (1978).
5. D. J. M. Bevan and S. E. Lawton, *Acta Crystallogr. B* **42,** 55 (1986).
6. J. P. Laval, A. Mikou, B. Frit, and J. Pannetier, *J. Solid State Chem.* **61,** 359 (1986).
7. M. P. van Dijk, F. C. Mijlhoff, and A. J. Burggraaf, *J. Solid State Chem.* **62,** 377 (1986).
8. P. D. Battle, C. R. A. Catlow, and L. Moroney, *J. Solid State Chem.* **67,** 42 (1987).
9. J. P. Laval, A. Mikou, B. Frit, and G. Roult, *Solid State Ionics* **28–30,** 1300 (1988).
10. T. Uehara, K. Koto, S. Emura, and F. Kanamaru, *Solid State Ionics* **23,** 331 (1987).
11. C. Keller, *in* "MTP International Review of Science" (K. W. Bagnall, Ed.), Vol. 7, Ser. 2, p. 1, Butterworths, London (1975).
12. H. Tagawa, T. Fujino, K. Ouchi, K. Watanabe, K. Saita, and T. Morimoto, *J. Nucl. Sci. Technol.* **20,** 467 (1983).
13. T. B. Lindemer and J. Brynestad, *J. Amer. Ceram. Soc.* **69,** 8678 (1986).
14. Y. Hinatsu and T. Fujino, *J. Solid State Chem.* **68,** 255 (1987).
15. H. G. Diehl and C. Keller, *J. Solid State Chem.* **3,** 621 (1971).
16. C. Keller, *in* "Gmelin Handbuch der Anorganishen Chemie," System-Nr55, U, TeilC, pp. 213–221, Springer-Verlag, Berlin/New York (1975).
17. Y. Hinatsu, N. Masaki, and T. Fujino, *J. Solid State Chem.* **73,** 567 (1988).
18. W. Rudorf, H. Erfurth, and S. Kemmler-Sack, *Z. Anorg. Allg. Chem.* **354,** 273 (1967).
19. L. M. Kovba, *Vestn. Mosk. Univ., Khim.* **13,** 341 (1972); C. A. **77,** 119202x (1972).
20. P. Herrero, R. M. Rojas, and P. Garcia, *Inorg. Chim. Acta* **140,** 159 (1987).
21. S. R. Dharwadkar and M. S. Chandrasekharaiah, *Anal. Chim. Acta* **45,** 545 (1969).
22. T. Fujino and T. Yamashita, *Fresenius' Z. Anal. Chem.* **314,** 156 (1983).
23. C. J. O'Connor, *in* "Progress in Inorganic Chemistry" (S. J. Lippard, Ed.), Vol. 29, p. 203, Wiley, New York (1982).
24. C. Keller and C. K. Jorgensen, *Chem. Phys. Lett.* **32,** 397 (1975).
25. C. Miyake, T. Isobe, Y. Yoneda, and S. Imoto, *Inorg. Chim. Acta* **140,** 137 (1987).
26. A. M. Chippindale, P. G. Dickens, and W. T. A. Harrison, *J. Solid State Chem.* **78,** 256 (1989).
27. B. W. Veal and D. J. Lam, *in* "Gmelin Handbuch der Anorganishen Chemie," System-Nr55, U, Teil A, p. 176, Springer-Verlag, Berlin (1980).
28. G. C. Allen, P. M. Tucker, and G. W. Tyler, *Vacuum* **32,** 481 (1982).
29. R. Delobel, H. Baussart, J. M. Leroy, J. Grimblot, and L. Gengembre, *J. Chem Soc., Faraday Trans. 1,* **79,** 879 (1983).
30. G. Allen, J. A. Crofts, M. T. Curtis, and P. M. Tucker, D. Chadwick, and P. J. Hampson, *J. Chem. Soc., Dalton Trans.,* 1296 (1974).
31. G. C. Allen, P. A. Tempest, and J. W. Tyler, *J. Chem. Soc., Faraday Trans. 1* **84,** 4049 (1988).
32. S. Kemmler-Sack, *Z. Anorg. Allg. Chem.* **363,** 295 (1968).
33. G. Gritzer and J. Selbin, *J. Inorg. Nucl. Chem.* **30,** 1799 (1968).
34. R. Brochu and J. Lucas, *Bull. Soc. Chim. Fr.* **12,** 4764 (1967).

35. G. C. ALLEN AND N. R. HOLMES, *J. Chem. Soc., Dalton Trans.*, 3009 (1987).
36. C. MIYAKE, S. OHANA, AND S. IMOTO, *Inorg. Chim. Acta* **140,** 133 (1987).
37. L. H. SCHWARTZ AND J. B. COHEN, *in* "Diffraction from Material," Chap. 7, Academic Press, New York (1977).
38. J. G. ALLPRESS AND H. J. ROSSELL, *J. Solid State Chem.* **15,** 68 (1975).
39. S. P. SINHA, *in* "Structure and Bonding," Vol. 25, p. 69, Springer-Verlag, Berlin/New York (1976).
40. A. F. WELLS, *in* "Structural Inorganic Chemistry," 5th ed., p. 482, Oxford Univ. Press, London/New York (1984).
41. A. F. WELLS, in "Structural Inorganic Chemistry," 5th ed., pp. 1268–1270, Oxford Univ. Press, London/New York (1984).